

In Vivo Apoptosis Imaging Using Site-Specifically ^{68}Ga -Labeled Annexin V

Matthias Bauwens

Abstract

Noninvasive molecular imaging, using positron emission tomography (PET), is an important technique to visualize metabolic processes in vivo. It also allows to visualize the process of apoptosis, by using radiolabeled compounds such as Annexin V, that bind to extracellular phosphatidylserine (PS). This chapter describes the radiosynthesis of ^{68}Ga -labeled Annexin V and how to noninvasively image apoptosis in vivo.

Key words Annexin V, ^{68}Ga , PET, Noninvasive imaging

1 Introduction

Apoptosis plays a role in a large number of diseases, such as neurodegenerative diseases, ischemic damage, autoimmune disorders, and many types of cancer. Timely assessment of in vivo apoptotic cell death in a particular tissue, for example in cancer tissue upon chemotherapeutic treatment, is of crucial importance to optimize treatment strategies, thereby improving patient survival and welfare. Classical techniques, such as computed tomography (CT) and magnetic resonance imaging (MRI), often require several months of treatment before a (relatively large-scale) anatomical effect can be seen [1]. Molecular imaging, on the other hand, can be performed within several days after the first treatment, showing a change in tissue metabolic rate. An even faster possibility is to visualize (apoptotic) cell death: this may allow to assess tumor cell death within one day [2, 3]. The general concept of molecular imaging (of apoptosis) requires radiolabeled compounds, also known as tracers, that can specifically bind to apoptotic cells, and with reasonable pharmacokinetics and biodistribution. Several radiolabeled apoptotic-targeting compounds have been developed for this purpose, with moderate success. The most well-known class of compounds is derived from Annexin V, targeting externalized

phosphatidylserine (PS), but other radiopharmaceuticals such as zinc dipicolylamine (also targeting PS), the Aposense family (targeting gamma-carboxyglutamic-acid (Gla)-domain proteins and intermembrane pH differences) and several others have also been described [4–8]. Numerous clinical trials with ^{99m}Tc -Annexin V have been performed, but widespread clinical application has not been achieved for various reasons [9–12]. Over the years, site-specifically radiolabeled analogues of Annexin V have been developed, where the radioisotope is specifically placed on a position of the Annexin, which is outside of the binding region, further improving the potential of radiolabeled annexin V [13, 14].

It is important to note that imaging apoptosis *in vivo* requires a relatively large degree of apoptosis in a tissue. In general, untreated tumors have a “background” level of apoptosis of 1–10 % (*see* Refs. 15 and 16 for examples), so visualizing a therapeutic effect requires a substantial short-term induction of apoptosis. This implies that drugs with long-lasting effects may not show noticeable efficacy when analyzed by imaging apoptosis at any particular time. Another confounding factor is necrosis: necrotic tissue (either from direct necrosis or through necroptosis) is very prevalent in cancer tissue, and also allows Annexin V to bind to “externalized” PS on exposed cell membranes.

This chapter focuses on the production and *in vivo* applicability of site-specifically ^{68}Ga -labeled Annexin V. The application is described both in an anti-Fas antibody mouse model and in a tumor bearing mouse model. The anti-Fas mouse model is a very straightforward method to induce fast and massive hepatic apoptosis (upto 70 % within 3 h), which can easily be visualized [17]. However, accumulation of pharmaceuticals in the liver (even those that do not induce any apoptosis) could lead to high level of false positives in this model. A tumor model, although more labor and time intensive, is better suited to fully analyze the properties of a radiopharmaceutical targeting apoptosis, as it mimics the human situation more closely. In this chapter we describe how to *in vivo* visualize apoptosis in a Burkitt’s lymphoma in mice, using established chemotherapy and radiotherapy. Of course, the technique also applies to any new chemotherapeutic apoptosis-inducing agent under investigation.

2 Materials

2.1 Equipment

1. Radiosynthesis module: a synthesis module, with sufficient shielding and suitable for handling ^{68}Ga , should be available. Manual synthesis, although technically possible, results in high radiation dose to the extremities and should be avoided. We used a module that was developed in-house, but commercial modules are available from several suppliers (*see* **Note 1**).

2. High Pressure Liquid Chromatography (HPLC): quality control is adequate by using an HPLC system with a UV detector at 254 nm and a 3-in. radiometric NaI(Tl) detector.
3. microPET: Focus 220 microPET device (Siemens). Alternatively, this may be another standalone device, or a combination with other imaging modalities (PET/CT, PET/MRI). Ideally, the microPET is equipped with monitoring apparatus for mouse health (temperature, respiratory rate).
4. MRI: small animal Bruker Biospec MR scanner (Bruker Biospin), operating at 9.4 T and using 3D Turbo RARE for image acquisition. The acquisition parameters for the 3D Turbo RARE experiment are as follows: a $256 \times 96 \times 96$ data matrix is acquired covering a field of view of $8 \times 3 \times 3$ cm, resulting in an isotropic resolution of 312 μm ; repetition time: 900 ms; effective echo time: 42 ms, RARE factor: 10; four dummy scans and one average. The total scan time is approximately 15 min.
5. Image analysis software: suitable software for analyzing μPET and μMRI images should be available. We use PMOD, but other programs are also suitable (AMIDE, ASIPRO, etc.).
6. Gamma-counter: automated NaI(Tl) gamma counter (we use Wallac 1480 Wizard 3", Perkin-Elmer).
7. Cryomicrotome: suitable for cutting 10–50 μm slices of tissues at -20 to -30 $^{\circ}\text{C}$.
8. Autoradiography device, including phosphor screens with a high spatial resolution (50 μm or better): Cyclone plus phosphor imager (Perkin-Elmer).
9. 10-kDa molecular weight cutoff (MWCO) filter unit, placed in a suitable centrifuge: a MWCO filter unit allows to filter any unlabelled ^{68}Ga from ^{68}Ga -labeled Annexin V (*see Note 1*).
10. pH paper and pH meter (*see Note 2*).

2.2 Solutions

All chemicals should be of analytical or pharmaceutical grade, unless otherwise mentioned. All solutions should be prepared freshly, stored at room temperature unless otherwise mentioned and used the same day.

1. $^{68}\text{Ge}/^{68}\text{Ga}$ generator: a $^{68}\text{Ge}/^{68}\text{Ga}$ generator of sufficient quality should be available. There are several suppliers at the moment, with minor differences in their output. The HCl-concentration required to elute ^{68}Ga from these generators differs in-between companies (ranging from 0.05 to 0.6 M), which will impact the concentration of buffer required in subsequent steps in order to reach a certain pH. In our case, ^{68}Ga was eluted with 0.6 M HCl.
2. Cys2-Annexin V: Obtained by site directed mutagenesis of the cDNA of human AnxA5, expressed in *E. coli* and purified to homogeneity (purity >95 %). More detailed production can be

found in Refs. 13 and 14 (*see Note 3*). 700 μg Cys2-AnxA5 corresponds to about 20 nmol.

3. Metal-free water: any water coming into contact with unbound ^{68}Ga should be as much as possible free of iron. This can be achieved by using doubly distilled or deionized water (milli-Q water), or by purchasing high-purity metal-free water (preferred) (*see Note 4*).
4. DOTA-maleimide (Macrocyclics, CheMatech, or similar companies in high quality): The DOTA functions as a chelator to trap the ^{68}Ga , while maleimide will bind to a free sulfur function (as in Cystein). Typically, we dissolve 0.8 mg in 1 ml of metal-free water and divide this into batches of 20 μl , which can be stored at $-20\text{ }^{\circ}\text{C}$ for upto 6 months.
5. 0.5 M sodium acetate buffer solution (pH 5.5): dissolve 4.1 g sodium acetate in 100 ml of metal-free water.
6. Hepes buffer: 25 mM Hepes, 40 mM NaCl: dissolve 0.595 g Hepes and 0.233 g NaCl in 100 ml milli-Q water.
7. 10 mM dithiothreitol solution (DTT): dissolve 15.4 mg in 10 ml milliQ water in a fumehood.
8. 2.5M TRIS buffer: dissolve 3.03 g tris(hydroxymethyl)amino-methane (TRIS) in 10 ml milli-Q water.
9. Purified hamster anti-Fas mAb (Dose: 0.2 μg of anti-Fas mAb per gram mouse, to be injected i.v.). Store at $4\text{ }^{\circ}\text{C}$ (*see Note 5*).

2.3 Animals

1. The mouse model is highly dependent on the type of research a scientific center is focusing on, but should be a well-established model and free of (mouse and human) pathogens. In our case, we work with NMRI mice or Severe Combined Immune Deficient (SCID)-mouse (C.B-17/Icr scid/scid) (Harlan) [18]. Maintenance of SCID mice is done in specific pathogen-free rooms with a high degree of protection, and according to national and international legislation.
2. Tumor-bearing mice: we use a human B-lymphoblast cell line Daudi, derived from a Burkitt's lymphoma. Upon inoculating $5 \cdot 10^5$ cells (in 200 μl PBS) subcutaneously near each shoulder, it takes 5–6 weeks for an approximately 1 ml size tumor is reached (*see Note 6*). These tumors have a background degree of apoptosis of 1–5 %, which can be increased manifold by adequate chemotherapy or radiation therapy.

3 Methods

3.1 Radiosynthesis

1. Production of ^{68}Ga -DOTA-maleimide.
 - Adjust the pH of the ^{68}Ga eluate to $\text{pH } 4 \pm 0.5$ by addition of 350 μl of a 3 M sodium acetate buffer solution.

- Add 20 nmol DOTA-maleimide (20 μ l of a 1 mg per ml solution) (this can be increased to 25 nmol if yields are unsatisfactory).
 - Heat mixture at 90 °C for 8 min and subsequently cool to room temperature.
 - Adjust pH to 7–7.5 by addition of 150 μ l of a 2.5 M TRIS buffer (pH 11.2).
2. Production of ^{68}Ga -DOTA-maleimide-Annexin V (^{68}Ga -AnxV).
- Add 250 μ l DTT solution to a solution of 700 μ g Cys2-AnxA5 in 250 μ l Hepes buffer to reduce any intermolecular disulfide bridges.
 - Incubate for 2 h at 37 °C and then apply to a 10-kDa MWCO filter unit (500 μ l capacity). Centrifuge at 12,000 $\times g$ for 15 min.
 - Wash the protein retained on the filter five times by centrifugation with 200 μ l of a Hepes buffer (5 min centrifugation) to remove the reductant and subsequently recover and transfer into 200 μ l Hepes buffer. About 80 % of the protein can be recovered, the remaining 20 % is lost due to stickiness to the filter unit (*see Note 7*).
 - Add the reduced Cys-AnxA5 to the ^{68}Ga -DOTA-maleimide and heat for 15 min at 37 °C.
 - Purify by applying the entire sample onto a 10-kDa MWCO filter unit (20 ml capacity) and centrifuging for 5 min at 3220 $\times g$. After washing with 2 ml Hepes buffer and again centrifuging once, the purified ^{68}Ga -Cys*-AnxA5 can be recovered in 200–300 μ l of Hepes buffer. Losses due to adsorption to the filter unit are typically about 10 % (*see Note 7*).

3.2 PET Imaging

1. Anti-Fas mouse model.

- Sedate NMRI mice with isoflurane anesthesia (2.5 % for induction and 1.0–1.5 % in O₂ for maintenance during scanning).
- Inject mice in a tail vein with purified hamster anti-Fas mAb (0.2 μ g/g of anti-Fas mAb, dissolved in 200 μ l PBS) (treated group) or with 200 μ l PBS (control group). Allow the mice to wake up and roam freely in an individual cage for 90 min, with access to water but not food.
- Sedate the mice again using isoflurane, and inject the mice via the tail vein with 7–15 MBq of ^{68}Ga -Cys2-Anx (*see Note 8*).
- Acquire dynamic images of the tracer distribution with the small animal PET camera for 60 min, keeping the liver in the center of the field of view. We use 12 times 5 s, 6 times 10 s, 6 times 30 s, 5 times 1 min, and 10 times 5 min as acquisition time frames. MRI imaging is optional, but not required.

- Sacrifice the animals using an overdose of pentobarbital or other suitable means. Take a 100 µl blood sample and dissect and weigh organs of interest. Measure the activity in an automated gamma counter to calculate the percentage of injected dose in each organ.
2. Burkitt's lymphoma mouse model.
- Inject cyclophosphamide (125 mg/kg) (treated group) or PBS (control group) intraperitoneally 1 day before µPET scanning (no sedation needed) [19].
 - Irradiate the tumors of mice in the treated group upto 10 Gy per tumor 4–6 h before µPET scanning (sedation using isoflurane) [20].
 - At the start of the µPET imaging experiment, sedate the mice with isoflurane anesthesia (2.5 % for induction and 1.0–1.5 % in O₂ for maintenance during scanning).
 - Inject the mice via the tail vein with 7–15 MBq of ⁶⁸Ga-Cys2-Anx.
 - Acquire dynamic images of the tracer distribution with the small animal PET camera for 60 min, keeping the tumor in the center of the field of view.
 - Immediately after the PET scan, perform the MRI scan. Make sure to not change the position of the animals by using a dedicated transportable mouse bed.
 - Sacrifice the animals using an overdose of pentobarbital or other suitable means. Take a 100 µl blood sample and dissect and weigh the tumor and organs of interest. Quickly measure the activity of the tumor in an automated gamma counter, then measure the other organs to calculate the percentage of injected dose in the tumor and each organ.
 - After measuring the radioactivity in the tumor, quickly freeze the tumor using isopentane in a bath of dry ice or by snap freezing (*see Note 9*). Cut sample into 10–50 µm slices at –25 °C, process slices for autoradiography, TUNEL, or H and E staining according to manufacturers' guidelines (*see Note 10*).
3. Image analysis.
- In vivo mages are analyzed using PMOD software, by fusing PET and MRI images using manual coregistration. MRI images are used for organ and tumor delineation, while superimposed PET images are used to interpret tracer accumulation (*see Fig. 1*).
 - Autoradiography images are matched to and compared with TUNEL and H and E staining. Heterogeneous uptake is very frequent (*see Fig. 2*).

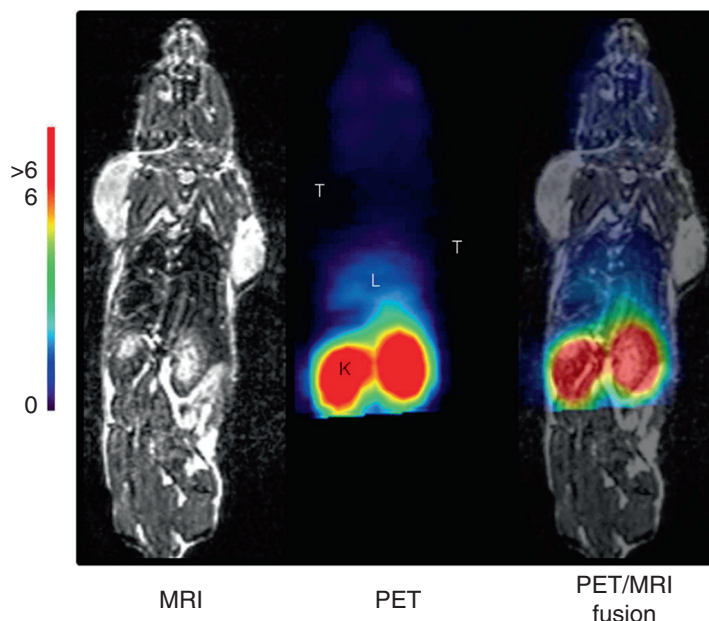


Fig. 1 MRI, PET, and PET/MRI image of a treated tumor-bearing mouse. The kidneys (**K**) are clearly visible on both MRI and PET images, as is the liver (**L**). The tumors cannot be distinguished on the PET image, but are clearly visible on the MRI image allowing delineation of the tumors. The scale indicates the intensity of the radioactive signal and is expressed as an SUV value (Standardized Uptake Value, radioactivity in Bq per volume in the region of interest, divided by the total amount of injected dose and multiplied by the animal weight)

4 Notes

1. Radiation protection is not to be underestimated in case of ^{68}Ga . For example, a dose of 100 MBq, at a distance of 30 cm (for example with an unshielded source on a bench), yields a dose of 0.2 mSv per hour. Knowing that a ^{68}Ga -generator can typically deliver up to 1500 MBq, the legal limit of 20 mSv per year is easily reached if inadequate protection is applied. Fully shielding ^{68}Ga (stopping more than 99 % of radiation) requires more than 5 cm of lead, which is difficult to achieve in practice around large equipment such as centrifuges.
2. Although a pH meter is more accurate, pH paper is preferred when measuring the pH of radioactive samples, as pH meters consistently become contaminated with radioactivity, rendering them unfit for other work.
3. The purity of the Annexin V preparation should be as high as possible, both in terms of protein purity and in absence of low molecular weight impurities such as DTT. For example, an equimolar presence of cysteine or DTT in comparison to the

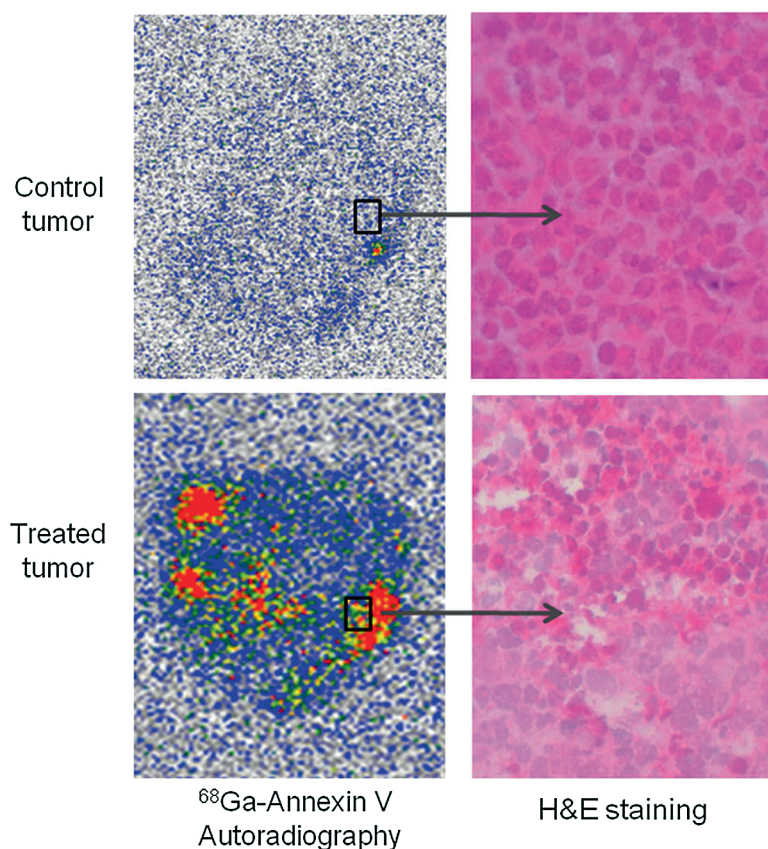


Fig. 2 Autoradiography (*left*) and H and E staining (*right*) slices of control (*top*) and treated (*bottom*) tumors. Note the heterogeneous uptake of ⁶⁸Ga-Annexin V, indicating heterogeneity of the degree of apoptosis within the tumor (confirmed by staining)

protein, may not show on routine protein purity analysis, but will dramatically reduce the yield of the radiosynthesis. When in doubt, perform an additional dialysis or centrifugal filtration over a MWCO filter prior to radiosynthesis.

4. Iron behaves very similar to gallium in many ways, including binding to chelators such as DOTA. Considering the low amount of ⁶⁸Ga (10^9 Bq corresponds to about 10 pmol), iron contaminations even from using metal spatula can be very disruptive to the radiochemical yield.
5. While storage of anti-Fas mAb should be done at 4 °C, care should be taken to warm up the antibody to at least room temperature (and preferably 37 °C) prior to i.v. injection for optimal animal comfort.
6. The location of the tumor is important: while tumors generally develop better when inoculated subcutaneously in the abdomen

region, such a location renders imaging more difficult as the clearance pathway of radiopharmaceuticals, either renally or hepatically, would be in too close proximity to the tumor. Alternative locations, such as near the shoulders or in the femur region, are therefore preferred. Additionally, care should be taken to use tumors with only minor amounts of necrosis: necrotic tissue is not well perfused (hampering uptake of the ^{68}Ga -Anx) and necrotic cells also present exposed PS, which is indistinguishable from extracellular PS as seen in apoptotic cells.

7. The stickiness to the filter can be reduced by washing the filter with PBS prior to administration of the compound.
8. The injection of the radiopharmaceutical should be done via a catheter, to allow fast and easy administration (reducing radiation dose to the technician) and to reduce the amount of paravenous injection.
9. Avoid placing the tumor directly in liquid nitrogen. In our experience, this results in brittle tissue, which is difficult to cut in the microtome.
10. Thicker slices allow for more radioactivity in the slice, enhancing autoradiography data, while thinner slices allow for better staining. Instead of going for an average thickness, it is best to alternatively cut 10 and 50 μm slices for each purpose.

Acknowledgements

This work was financially supported by the European Union through the grant Euregional PACT II by the Interreg IV program of Gensregio Vlaanderen-Nederland (IVA-VLANED-1.20) and the Center of Excellence “MoSAIC” of the K.U. Leuven.

References

1. Therasse P, Arbuck SG, Eisenhauer EA, Wanders J, Kaplan RS, Rubinstein L, Verweij J, Van Glabbeke M, van Oosterom AT, Christian MC, Gwyther SG (2000) New guidelines to evaluate the response to treatment in solid tumors. European Organization for Research and Treatment of Cancer, National Cancer Institute of the United States. *J Natl Cancer Inst* 92(3):205–216
2. Neves AA, Brindle KM (2006) Assessing responses to cancer therapy using molecular imaging. *Biochim Biophys Acta* 1766(2): 242–261
3. De Saint-Hubert M, Prinsen K, Mortelmans L, Verbruggen A, Mottaghy FM (2009) Molecular imaging of cell death. *Methods* 48(2):178–187
4. Koulov AV, Stucker KA, Lakshmi C, Robinson JP, Smith BD (2003) Detection of apoptotic cells using a synthetic fluorescent sensor for membrane surfaces that contain phosphatidylserine. *Cell Death Differ* 10(12):1357–1359
5. Cohen A, Ziv I, Aloya T, Levin G, Kidron D, Grimberg H, Reshef A, Shirvan A (2007) Monitoring of chemotherapy-induced cell death in melanoma tumors by N, N'-Didansyl-L-cystine. *Technol Cancer Res Treat* 6(3):221–234
6. Aloya R, Shirvan A, Grimberg H, Reshef A, Levin G, Kidron D, Cohen A, Ziv I (2006) Molecular imaging of cell death *in vivo* by a

- novel small molecule probe. *Apoptosis* 11(12):2089–2101
7. Zeng W, Wang X, Xu P, Liu G, Eden HS, Chen X (2015) Molecular imaging of apoptosis: from micro to macro. *Theranostics* 5(6):559–582
 8. Ogawa K, Aoki M (2014) Radiolabeled apoptosis imaging agents for early detection of response to therapy. *Sci World J* 2014:732603
 9. Yang TJ, Haimovitz-Friedman A, Verheij M (2012) Anticancer therapy and apoptosis imaging. *Exp Oncol* 34(3):269–276
 10. Blankenberg FG, Katsikis PD, Tait JF, Davis RE, Naumovski L, Ohtsuki K, Kopiwoda S, Abrams MJ, Strauss HW (1999) Imaging of apoptosis (programmed cell death) with ^{99m}Tc annexin V. *J Nucl Med* 40(1):184–191
 11. Hofstra L, Liem IH, Dumont EA, Boersma HH, van Heerde WL, Doevendans PA, De Muinck E, Wellens HJ, Kemerink GJ, Reutelingsperger CP, Heidendal GA (2000) Visualisation of cell death *in vivo* in patients with acute myocardial infarction. *Lancet* 356(9225):209–212
 12. Vangestel C, Peeters M, Mees G, Oltenfreiter R, Boersma HH, Elsinga PH, Reutelingsperger C, Van Damme N, De Spiegeleer B, Van de Wiele C (2011) *In vivo* imaging of apoptosis in oncology: an update. *Mol Imaging* 10(5):340–358
 13. De Saint-Hubert M, Mottaghy FM, Vunckx K, Nuyts J, Fonge H, Prinsen K, Stroobants S, Mortelmans L, Deckers N, Hofstra L, Reutelingsperger CP, Verbruggen A, Rattat D (2010) Site-specific labeling of ‘second generation’ annexin V with $^{99m}\text{Tc}(\text{CO})_3$ for improved imaging of apoptosis *in vivo*. *Bioorg Med Chem* 18(3):1356–1363
 14. Bauwens M, De Saint-Hubert M, Devos E, Deckers N, Reutelingsperger C, Mortelmans L, Himmelreich U, Mottaghy FM, Verbruggen A (2011) Site-specific ^{68}Ga -labeled Annexin A5 as a PET imaging agent for apoptosis. *Nucl Med Biol* 38(3):381–392
 15. Sakaguchi Y, Stephens LC, Makino M, Kaneko T, Strebel FR, Danhauser LL, Jenkins GN, Bull JM (1995) Apoptosis in tumors and normal tissues induced by whole body hyperthermia in rats. *Cancer Res* 55(22):5459–5464
 16. Tan S, Peng X, Peng W, Zhao Y, Wei Y (2015) Enhancement of oxaliplatin-induced cell apoptosis and tumor suppression by 3-methyladenine in colon cancer. *Oncol Lett* 9(5):2056–2062
 17. Feldmann G, Lamboley C, Moreau A, Bringuier A (1998) Fas-mediated apoptosis of hepatic cells. *Biomed Pharmacother* 52(9):378–385
 18. Ghetie MA, Richardson J, Tucker T, Jones D, Uhr JW, Vitetta ES (1990) Disseminated or localized growth of a human B-cell tumor (Daudi) in SCID mice. *Int J Cancer* 45(3):481–485
 19. Takei T, Kuge Y, Zhao S, Sato M, Strauss HW, Blankenberg FG, Tait JF, Tamaki N (2004) Time course of apoptotic tumor response after a single dose of chemotherapy: comparison with ^{99m}Tc -annexin V uptake and histologic findings in an experimental model. *J Nucl Med* 45(12):2083–2087
 20. Mirkovic N, Meyn RE, Hunter NR, Milas L (1994) Radiation-induced apoptosis in a murine lymphoma *in vivo*. *Radiother Oncol* 33(1):11–16

Programmed Cell Death

Methods and Protocols

Puthalakath, H.; Hawkins, C. (Eds.)

2016, XI, 291 p. 59 illus., 39 illus. in color. With online files/update., Hardcover

ISBN: 978-1-4939-3579-6

A product of Humana Press